Interplay between the potential waveform and diffusion layer dynamics determines the time-response of voltammetric detection in microchannels

Raphaël Trouillon[1,a,*] and Martin A. M. Gijs[a]

[a] Laboratory of Microsystems, Ecole Polytechnique Fédérale de Lausanne, CH-1015 Lausanne, Switzerland; raphael.trouillon@m4x.org; tel: +41 (0)2169 36584

[*] Corresponding author

[1] Member of the ISE

The diffusion layer is a critical factor affecting the temporal response of electrochemical devices. In this article, we have investigated the effect of the relaxation of the diffusion layer during the potentiodynamic sensing of ferrocenemethanol (FcMeOH) in microchannels and compared these results to amperometry. First, the effect of the relaxation of the diffusion layer is described, both theoretically and experimentally. Then, chronoamperometric and voltammetric measurements were considered, and the rate of current increase as a plug of FcMeOH is injected into the device was studied for both cases. It was found that, for the oxidation of FcMeOH, the waveform maximising the duration of the anodic phase provided an improved response for potentiodynamic methods, even though amperometry was always found to show the best results. This was further established by extracting the impulse and modulation transfer functions, which characterize the time and frequency responses, respectively, of the fluidic/ electrochemical system. These findings can help designing potential waveforms improving the time response of the device, in systems where high temporal resolution is needed. This is particularly appropriate to bioelectrochemical analyses, where release and uptake phenomena can occur on the millisecond timescale.

Keywords: microfluidics; diffusive relaxation; time response; amperometry; voltammetry

1. Introduction

Electrochemical methods are strong candidates for on-chip chemical analysis [1–3]. Indeed, contrary to many analytical techniques, electrochemical sensors are highly amenable to miniaturization and can be easily batchproduced with standard microfabrication techniques [4–6]. They are also attractive solutions for cheap, hand-held measurement systems applicable for instance to point-of-care diagnostics [7,8]. However, the specificity of electrochemical sensing, where the reaction actually induces

a gradient of analyte established at the electrode following Fick's laws, requires a careful characterization of the detection system, especially if it is embedded into a microfluidic circuit. Indeed, several reports have highlighted the specific behaviour of electrochemistry in microchannels [9–13], where the mass transport characteristics are radically different from the ones encountered in traditional conditions of electrochemistry [14–16]. The fast time response and sensitivity of electrochemical sensors is one of their most attractive features, allowing for example the detection of neuronal transmission [17–22] or single molecules [23,24]. The effects of convection and diffusion on the temporal behaviour of electrochemical sensors therefore have to be studied carefully for these devices.

Amperometry (AMP) is considered as one of the electrochemical methods providing the highest time response. In contrast, cyclic voltammetry (CV), or other potentiodynamic techniques, are popular because of its improved chemical resolution, allowing for the simultaneous quantitation of different analytes. In a previous report [25], we have compared the response of AMP and CV to the injections of a plug of 1 mM ferrocenemethanol (FcMeOH) in a microfluidic system. This redox probe was used because of its fast electron transfer [11,26,27], guaranteeing that the observations will arise from mass transport rather than secondary reactions (adsorption, formation of chemical bonds…). In addition, its oxidation occurs at a potential where the results will not be distorted by oxygen reduction (oxygen is technically hard to remove from poly-dimethylsiloxane (PDMS) chips). This system (Fig. 1A) featured a fluidic chip allowing the injection of two different streams of liquid (typically, buffer and analyte), which are then mixed through several serpentines (channel height: 100 µm), before entering a sensing chamber (Ø 1 mm). This chamber contained a Pt working electrode (WE) positioned along its vertical axis. The system is completed with an aqueous Ag|AgCl (3 M KCl) reference electrode (RE). The small size of the microchannels induced a high solution resistance, and the expected iR drop in this two-electrode configuration is in the 1-10 mV range. Furthermore, the faradaic currents observed during the experiments are ~100 nA, and in principle could induce a polarization of the reference electrode. This polarization is however expected to be limited because of the large effective surface of the chlorinated silver wire, with respect to the area of the WE, thus resulting in a lower current density at the surface of the RE. Furthermore, in all the experiments, the current of interest was measured in the diffusion-limited regime, and the applied overpotential was high enough not to be hindered by small variations of the RE due to an eventual iR drop or electrode polarization. The Reynolds' number in the microchannels section of the chip is ~100 at the highest flow rate considered (10 µl s^{-1}). In all the cases considered previously for the detection of plugs of FcMeOH in microchannels [25], the CV response was delayed over the AMP traces. As FcMeOH was found to show outer-sphere properties in our system, with a fast electron transfer, this delay was attributed to mass transport, more precisely to the relaxation of the diffusion layer in response to the observed concentration changes [28,29].

During electrochemical detection, the system establishes a diffusion layer of thickness δ_D in a region immediately adjacent to the electrode (for $0 \leq z \leq \delta_D$). Following a common approximation [30], if the system is positioned in a stream of fluid of flow rate v, this region is characterised by the absence of any significant convection, which allows the establishment of the diffusion layer, in agreement with the Prandtl's hypothesis [31], as shown in Fig. 1B. On the other hand, for $z > \delta_D$, the fluid is well-mixed by the convection field, and the analyte concentration can be approximated as uniform. Even though it is possible, for the sake of clarity,

to assume that there are only two discrete regions, one where diffusive transport controls the flux of analyte, and another one where convection dominates, and that the Prandtl's viscous boundary layer can be identified to the diffusion layer, the actual system is more complex. In our system, the Schmidt number *Sc*, the ratio of the kinematic viscosity to the diffusion coefficient, is high (>10^4), and the viscous boundary layer is expected to be much thicker than the diffusion layer, by a factor approximated with $Sc^{1/3}$ [32], which means in our device that the viscous boundary layer is at least 10 times thicker than the diffusion layer. In a linear approximation of the fluid velocity at the vicinity of the wall, the velocity at the edge of the diffusion layer would be, at best, a tenth of the maximal velocity in the chamber. This is in agreement with distinct domains where mass transport is respectively controlled by diffusion and convection. From the simulations shown in Supporting Information, it can be observed that, at the velocities considered in our system, the diffusion layer is indeed included into the viscous boundary layer, in an area where the fluid velocity is much lower than in the rest of the system. The steadystate thickness of the diffusion layer under hydrodynamic conditions (1 – 10 µl s^{-1}) was found to be few micrometers. For AMP measurements, the diffusion layer is continuously established, and any change in concentration is immediately detected thus leading to a fast response time. On the other hand, for CV, the geometry of this layer constantly changes as the electrode potential *E* is swept back and forth, consuming and regenerating the analyte. Hence, before the electrode can well access the value of interest, *i.e.* the bulk analyte concentration, the diffusion layer first has to be established, thus inducing a delayed response over AMP. This phenomenon is qualitatively and quantitatively similar to the delayed response observed in an RC circuit, the diffusion layer actually behaving as an RC component [25], that gives rise to a characteristic relaxation time τ_D in the signal [28,29]:

$$\tau_D = \frac{\delta^2}{2D} \quad (1)$$

where *D* is the diffusion coefficient. The relaxation time physically corresponds to the time required to build an analyte gradient across the diffusion layer in response to a perturbation in the system. When the diffusion layer has overcome its relaxation, we refer to a well-developed diffusion layer. However, despite this delayed response, CV is a powerful and important technique because of its higher chemical resolution, allowing multi-analyte sensing.

In this report, we investigate how the operating conditions can affect the relaxation of the diffusion layer and therefore the time response of potentiodynamic systems. More precisely, we study the impact of the potential waveform in chronamperometry (CA) and CV on the temporal response of electrochemical detection in a microfluidic device. The ratio of the durations of the oxidation and reduction phases in CA and CV is investigated, as this factor is expected to alter the profile of the diffusion layer. In the case of FcMeOH oxidation, it was found that CA or CV potential waveforms with the longest durations for the oxidation phase showed the fastest development of the diffusion layer and the best time response. Based on these results, it is then possible to establish optimised waveforms improving the response of potentiodynamic detection systems and to deconvolute the contribution of the relaxation of the diffusion layer from the experimental data.

2. Experimental

All the experiments were carried out with an Ivium Powerstat (Ivium, The Netherlands) functioning in the 2-electrode mode and performed in PBS as a supporting electrolyte. The reference electrode was an aqueous Ag|AgCl (3 M KCl) electrode, and all the potentials are reported vs Ag|AgCl. The fluid flows were actuated from a computer-controlled Nemesys system (Cetoni GmbH, Germany) featuring two low pressure pump modules. The CVs were run at a scan rate SR of 10 V s^{-1} (unless stated otherwise). The AMP traces were all recorded at 0.4 V vs Ag|AgCl for FcMeOH oxidation and -0.4 V vs Ag|AgCl for ruthenium hexaammine (III) reduction (RuHex). In both cases, the measured current *I* was background subtracted and normalised to its maximum value I_{max}. Depending on the experiment, the data presented corresponds to 5 Hz or 10 Hz sampling.

Additional details on the experimental procedures (fabrication of the chip, electrochemical measurements, data processing…) are provided in the Supporting Information.

3. Results and Discussion

3.1. Delayed response of voltammetric methods over amperometric detection

To further demonstrate the delayed response of CV with respect to AMP, the experiment detailed previously [25] for FcMeOH was repeated for the outer-sphere probe RuHex. A 4 s plug of 1 mM RuHex was injected (v= 10 µl s^{-1}) into a stream of PBS. CVs were performed at 10 V s^{-1}, from 0 to -0.5 V vs Ag|AgCl, corresponding to a 10 Hz sampling. The traces were all obtained from the same chip, and the data presented is the average of 4 traces obtained in identical conditions (see Supporting Information). This was done to avoid minute chip-to-chip variations which could hinder the frequency analysis performed on that data. The results are displayed in Fig. 1C, left. As expected, the delayed response of CV discussed above for FcMeOH is observed also for RuHex. The fact that this phenomenon is observed for the reduction of a different outer-sphere redox species confirms the results obtained with FcMeOH.

The IF and the MTF of FcMeOH (obtained from ref. [25]) and RuHex tests, for CV and AMP, are shown in Fig. 1C, center (IF) and right (MTF). These functions are indicative of the time response of the system (see Supporting Information). Interestingly, the MTF of AMP and CV are similar for RuHex and FcMeOH. As the *D* of FcMeOH ((7.6 ± 0.4) 10^{-10} m^2 s^{-1}) [12] and RuHex ((5.5 ± 0.2) 10^{-10} m^2 s^{-1}) [33] are close, this further establishes the idea that the delayed response of CV is based, in this specific case, on mass transport rather than analyte/ electrode interaction. In other words, in this case, the shape of the MTF is solely determined by the diffusive/ convective properties of the system in the case of fast electron transfer.

Even though the contribution of oxygen reduction could be adequately removed from the measured signal during the RuHex analysis, FcMeOH was preferred for the following analysis. Indeed, some of experiments involved a significant extension of the potential range scanned during CV (*vide infra*). In the case of RuHex, the extension of the cathodic limit would have increased the contribution of oxygen reduction to the measured signal, potentially distorting the result.

This was not expected to happen with FcMeOH.

3.2. Effect of the diffusion layer relaxation during cyclic chronoamperometry

The delayed response of CV, and more generally the temporal resolution of electrochemical methods being influenced by the dynamics of the diffusion layer, hints that the profile of the input potential waveform may also alter the quality of electrochemical detection, precisely by modifying the geometry of the diffusion layer, all the other experimental parameters being kept unchanged. To investigate this, several repeated CA cycles of duration t_c= 100 ms (see Fig. 2A) have been run to obtain cyclic CA data. This analysis was performed in a quiescent (v= 0 µl s^{-1}) solution of 1 mM FcMeOH, and a single cycle consisted in an oxidation phase (0.4 V vs Ag|AgCl), followed by a reduction phase (0.1 V vs Ag|AgCl), as highlighted in Fig. 2B. These two potentials were chosen in the diffusion-limited regions of the CV curve obtained for FcMeOH (Fig. 2C), and were chosen to ensure the observed phenomena are mainly associated to mass transport. The signal of interest was the current at the end of the oxidation phase, as shown by the black dots on Fig. 2A. The parameter we used for our analysis was the ratio η, quantifying the fraction of the 100 ms cycle during which FcMeOH is oxidised at the electrode:

$$\eta = \frac{t_{ox}}{t_{ox}+t_{red}} = \frac{t_{ox}}{t_c} \quad (2)$$

where t_{ox} and t_{red} are respectively the duration of the oxidation and reduction phases during a single CA cycle (Fig. 2B). As shown on Fig. 2A, and to facilitate data analysis, the experiment was preceded by a reduction phase, of duration t_{red}, so that all the current points of interest are exactly localised at multiples of t_c.

The purpose of our analysis is to investigate the effect of η on the dynamics of the concentration profile, and hence on the measured current, during cyclic CA. Kambara suggested the use of the principle of superposition to compute the concentration and CA current profiles during changes of potential [34]. Roughly, the successive steps of potential can be associated to discontinuous concentration profiles and several sets of initial conditions and differential equations. These equations can be solved independently, and the different resulting concentration profiles can be added to obtain the final solution of the system. For instance, in the case of a single CA cycle consisting in an oxidation step followed by a reduction step (*i.e.* for $0 \leq t \leq t_c$ as shown in Fig. 2B), using the notations detailed above:

$$c(z,t) = c_0^* \operatorname{erf}\frac{z}{2\sqrt{Dt}} \quad \text{for } t \leq t_{ox}$$

$$= c_0^* \operatorname{erf}\frac{z}{2\sqrt{Dt}} + \operatorname{erfc}\frac{z}{2\sqrt{D(t-t_{ox})}} \quad \text{for } t > t_{ox} \quad (3)$$

where $c(z,t)$ is the concentration of the analyte of interest (here, FcMeOH) as a function of time and z, the normal distance to the electrode surface, c_0^* is the bulk concentration of FcMeOH and *erf* and *erfc* are respectively the error and complementary error functions. This equation shows that the concentration profile initiated during the oxidation phase is still evolving and spreading during the reduction phase.

Using this solution, the profiles for $c(z,t)$ over this single CA cycle were computed for η= 0.2 and η= 0.8, as shown in Fig. 2D. From these simulations, it appears that for low η values, the system is brought back to its initial state at the end of the cycle, with a

uniform FcMeOH concentration at the vicinity of the electrode close to ~c_0^*. However, for high values of η, a residual gradient of concentration in the z-direction can still be observed at the end of the cycle. This artefact will hinder the analyte diffusion during the following cycle, leading to a lower recorded current during the oxidation phase than for a small η. The relaxation of the diffusion layer, which characterizes the time needed to respond to a perturbation and obtain a well-developed diffusion layer, is here directly observed as hindering the electrochemical response, especially at high scanning frequency, by preventing the fast actuation of the diffusing analytes.

Interestingly, the superposition method used by Kambara to obtain eqn. (3) can be extended to calculate the current response at the end of the oxidation phase of the successive CA cycles too. This is simply performed by differentiating eqn. (3) with respect to time and adding cumulatively the variations corresponding to each cycle [34]. The result of this method is presented in Supporting Information. Overall, the calculations suggest that the measured current I may vary linearly with $1/\sqrt{(n-1)t_c} \approx 1/\sqrt{t}$ (cf. eqn. (S3), see Supporting Information) where n is the number of cycles. The system is expected to asymptotically converge towards a steady-state, defined by the difference of the two Riemann's series defined in Supporting Information, showing that this equilibrium actually arises from the competition of the oxidation and reduction phases of the cyclic CA. Also, the linear slope computed when the current is plotted *vs.* $1/\sqrt{t}$ should be proportional to t_{ox} and therefore to η as t_c is fixed.

Fig. 3A-C shows the theoretical results obtained from this model, assuming a cyclic CA analysis in a quiescent (v= 0 µl s^{-1}) solution of 1 mM FcMeOH. As stated before, t_c was fixed at 100 ms, and the current corresponding to the end of the oxidation phase, for each cycle, was computed using eqn. (S1) in Supporting Information, for a potential waveform corresponding to our experimental conditions (Fig. 2A). Furthermore, to allow direct comparison of the traces, and cancel any scaling effect that could be due to variations in electrode size or geometry, the obtained current was normalized to its maximal value (*i.e.*, the one obtained for t= 100 ms). The special case where η=1 (i.e. no reduction phase, which corresponds to AMP) was also considered. Immediately, from eqn. (S1) (see Supporting Information), the successive terms of the sum cancel each other for η=1, so that the potential waveform actually corresponds to the one of a standard AMP analysis, and the response is described by the Cottrell equation [30]. Fig. 3A displays the normalized currents, *vs.* time, for different η. As expected, the normalized currents are almost constantly equal to 1 for small η values, and decrease sharply otherwise. If the same data is plotted *vs.* $1/\sqrt{t}$, a clear linear behaviour is observed (Fig. 3B), as expected from eqn. (S3). Furthermore, the slope α of these linear curves is proportional to $\eta^{3/2}$ (Fig. 3C). Indeed, the slopes obtained from eqn (S3) are proportional to η. Additionally, the current has been normalized by $i_1 = 1/\sqrt{t_{oo}}$ (see Supporting Information) and which is proportional to $\eta^{-1/2}$ as detailed above. Hence, the slopes of the curves shown on Fig. 3B are expected to be proportional to $\eta^{3/2}$, in agreement with our simulation.

To confirm this model, experimental data was obtained from our fluidic/ electrochemical system (1 mM FcMeOH in PBS, v= 0 µl s^{-1}). The effects of the discharge currents generated by the RC constant of the electrode surface were here not considered because of the small (~0.2 ms) RC constant previously calculated for this type of device [25]. The results for the normalized currents are shown in Fig. 3D (average of N= 4 chips), and are in good agreement with the theory. Furthermore, and especially for low η values,

the currents seem to be converging towards a steady-state over the course of the experiment, as expected from the calculations shown in Supporting Information. However, for η>0.4, the current decay is faster for the model than for the experimental data. This could be an indication of residual baseline currents that were not taken into account in the model. This was not considered as a critical issue, as only the timedependent decay of the current is significant in our analysis. Moreover, the data fits with the CA model, thus validating this approach. Indeed, the experimental data linearly increase with $1/\sqrt{t}$ (Fig. 3E, N= 4 chips), and the α values obtained from these curves are proportional to $\eta^{3/2}$ (Fig. 3F).

Overall, our theoretical analysis is in good agreement with the observed experimental response of cyclic CA. Interestingly, the fact that the current is linearly dependent on $1/\sqrt{t}$ immediately hints that the current response, sampled from the end of the oxidation phase, can be simply modelled with the Cottrell equation [30]. In contrast to the Cottrell equation, the establishment of the diffusion layer is here slowed by the partial regeneration of the analyte during the reduction phase. The responses of the two systems differ only by a constant multiplication with a term accounting for the regeneration of the analyte. Studying the cyclic CA system is therefore similar to tracking the progression of the diffusion layer, whose thickness is proportional to $1/\sqrt{t}$ and grows faster for high η values.

More importantly, these results show that, despite the cyclic nature of the potential waveform, the response for a given time is strongly influenced by the previous cycles. This is because of the non-zero relaxation time of the diffusion layer, and the system is not fully brought back to its initial state at the end of each cycle. This is expected to alter the time response of the system, as shown below.

3.3. Effect of η on the time response of cyclic CA detection

The cyclic CA analysis showed that the η factor induced different responses in quiescent solutions, all the other experimental parameters being strictly identical. For high η values, the longer oxidation time will induce a faster development of the diffusion layer, as shown from Fig. 3E and the slopes α in Fig. 3F. Qualitatively, as η increases towards 1, the response of the system should approach the one of AMP, and the time response of the device should be improved. To investigate this, the response of cyclic CA to the injection of plugs of FcMeOH was studied.

As previously described, the fluidic part of our chip was used to inject, for 4 s, plugs of 1 mM FcMeOH. In this case, v= 5 µl s^{-1}. This low flow velocity ensured that we could test ten different η of interest without refilling the input syringes, so that all the traces could be obtained in identical conditions. Fig. 4A shows three background-subtracted, normalized traces (η= 0.1, 0.5 and 1) corresponding to the injection of a 4 s plug (average of N= 3 chips). As expected, the time response is improved as η increases. This fact already shows that, all the other parameters being equal, the relative duration of the oxidation regime, which characterizes the establishment of the diffusion layer, in comparison to the reduction phase, alters the temporal response of electrochemical methods.

Similar curves where obtained for different η values (η= 0.1, 0.2 … 1). As discussed in a previous report [25], the rising part of the current curves, corresponding to the onset of the concentration plug, is well-fit with the positive part of *erf* (i.e., for t>0s). This function is known to describe the diffusive variations of the concentration, as shown in eqn. (3) [35].

The curves of Fig. 4A were therefore fit with:

$$ccffcnt(t) = a\ \mathrm{erf}\frac{t}{\sigma\sqrt{2}}\ \mathrm{if\ t} > 0\ \mathrm{s}$$

$$= 0\ fthcfeiec \qquad (4)$$

where a is a fitting parameter. The parameter σ is the standard deviation of the Gaussian integrated in the definition of the error function, and is here characteristic of the broadening induced by Taylor dispersion and electrochemical delayed response [25]. A low σ value is indicative of a sharp current rise, and therefore of a better temporal resolution. Each experimental curve was fit with this function, and the obtained values for σ were extracted and displayed in Fig. 4B (N= 3 chips, average ± SD). A clear linear decay is observed with increasing η, showing that, as the oxidation phase becomes more prevalent, the temporal resolution of the detector is improved.

One could argue that the faster response in the case of the high η could possibly arise from a thicker diffusion layer. Indeed, the fluid velocity is decreased linearly in the viscous boundary layer. Then, in this region, the changes in concentration actuated by the syringe pumps should be less rapid close to the walls of the channel than in a region of the system closer to the center of the channel where the velocity is maximal. Hence, for high η ratios, the diffusion layer could grow thick enough to reach such parts of the system with higher fluid velocities, where the concentration variations are steeper, resulting in enhanced time resolutions. However, as explained above, the diffusion layer is largely limited by the Prandtl's layer. The system should therefore be constrained to the same region and consequently exposed to similar fluid velocities and concentration profiles, for each η.

As a result, this phenomenon probably arises from the relaxation time of the diffusion system and is both qualitatively and quantitatively similar to the initial stabilization of an RC system in electronics, leading to a transient regime and then to a steady-state allowing analysis. As reported before [25], τ_D was calculated as being few tens of ms for this system, in this range of v. In our experimental setup, depending on the value of η, t_{red} and t_{ox} are in the 0 to 100 ms range and can be lower of higher than τ_D. At low η values, t_{red} is long and t_{ox} is short. By following the analogy with an RC system in electronics, the characteristic time of the input signal (here, t_{ox}) is smaller than the relaxation time of the system. Therefore, the high frequency components of the system will be filtered out as the diffusive system will function as a low-pass filter of characteristic time τ_D. On the other hand, for high η values, t_{red} is short and t_{ox} is long and can exceed τ_D. This will result in a well-developed diffusion layer in equilibrium with the viscous boundary layer, as explained in the Introduction. Furthermore, the perturbation introduced by the reduction phase is very short, and will therefore be filtered off by the relaxation phenomena. Therefore, the diffusion layer is largely well-developed, apart from the small disturbances occurring during the reduction phase, and approaches the AMP detection modality, hence explaining the higher temporal resolution obtained for high η values.

3.4. Effect of the range of potentials scanned on the time response of CV detection

In the previous sections, the cyclic CA method was actually used as a technique to understand what happens during repeated CV cycles. In both CA and CV, oxidation alternates continuously with reduction, but in the case of cyclic CA, the theory and equations describing the current variations are much simpler, as we have chosen our step potentials in only two diffusion-limited points of the CV curves. In this section, an additional analysis is carried out on traces obtained from AMP and CV. The electrochemical response was always measured at the same potential (0.4 V vs Ag|AgCl) both for CV and AMP.

To mimic the role of η from the previous sections, the range of potentials swept during the CV scans was translated. As shown on Fig. 5A, three ranges of potential were considered: 0 to 1 V vs Ag|AgCl, -0.25 to 0.75 V vs Ag|AgCl and 0.5 to 0.5 V vs Ag|AgCl (note that, for that panel only, and to minimize the capacitive current, these CV traces were obtained for SR= 0.5 V s^{-1}). These three scan ranges have the same amplitude (1 V), t_{ox} and t_{red} can be obtained and approximate η ratios can therefore be attributed to each range: 0.78 (0 to 1 V vs Ag|AgCl), 0.53 (-0.25 to 0.75 V vs Ag|AgCl) and 0.28 (-0.5 to 0.5 V vs Ag|AgCl). For the actual plug detection experiment, the CVs were all scanned at 10 V s^{-1}, corresponding to a 5 Hz sampling rate (the AMP data was sampled at 10 Hz, but the dataset was reduced to correspond to a 5 Hz sampling for the analysis). Normalised and background-subtracted current traces were obtained for the three CV ranges and for AMP, for 4 s plugs of 1 mM FcMeOH injected at 10 µl s^{-1}. Here, the data was obtained from several repeats on the same chip to avoid inaccuracies due to chip-to-chip variations. The results are shown on Fig. 5B (average of N=4 repeats). As previously expected, AMP offers the best temporal response, as the recorded current rise is the sharpest because of its well-developed diffusion layer. Additionally, and in good agreement with the cyclic CA results, the potential range associated to the highest η offers the second fastest response. In general, the temporal response worsens as the potential range is translated towards negative values (i.e. as η decreases). Similarly, the IFs (Fig. 5C) and MTFs (Fig. 5D) associated to these traces show unambiguously that AMP offers the best performances, followed by the 0 to 1 V vs Ag|AgCl range, and that only high η values offer an increased temporal behaviour, in agreement with the CA analysis.

Overall, this section shows that our η analysis is also valid for CV measurements. Even though the width of the potential windows were the same, and the electrochemical response was always measured at the same potential (0.4 V) both for CV and AMP, the delayed response of CV for decreasing η values further stresses the importance of overcoming the relaxation of the diffusion layer to achieve reliable measurements of fast transients. A similar response has been observed for the voltammetric detection of serotonin [36].

Increasing the quality of electrochemical measurements by increasing the anodic upper limit of the potential scans, usually leading to an increase in η, has been previously reported [37–39]. In this case, where dopamine (DA) was the analyte of interest, this improved response was largely attributed to enhanced DA adsorption to the oxidised carbon electrode surface. In our case, even though structural changes in the Pt electrode surface could be expected (as indicated by the slight variations in capacitive current for the 0 to 1 V vs Ag|AgCl range in Fig. 5A), the fact that the studied analyte shows the characteristic of an outer-sphere specie in our setup ensures that the observed differences are mostly due to mass-transport rather than analyte/ substrate interactions. Additionally, the fact that the same behaviour (high η improves the response) is also observed for cyclic CA, where the potential

stays in a range where no change in the Pt surface is expected, further suggests that the observed phenomena arises from diffusion/ convection. Therefore, even though analyte adsorption is not studied in this report, it is expected that the improved response granted by a higher anodic limit during fast scan CV measurements is, at least in part, due to a more developed diffusion layer induced by the higher η value associated to the extended waveform. In the case of more complex electrochemical reactions, such as the oxidation of neurotransmitters, additional phenomena (analyte adsorption, changes in the electrode surface…) are also expected to contribute to the time response of the system.

3.5. Isolating the electrochemical delay from fluidic dispersion

As suggested by others [40], the frequency response of the system detailed previously can be used to cancel the signal distortion induced by the non-optimal profile (*i.e*. not a Dirac function) of the IF. This can be performed by deconvoluting the characteristic IF of the detector from the output signal. However, the IFs presented on Fig. 5C also contain some information related to the dispersion of the plug into the channel [35], in addition to the signal of interest arising from the electrochemical detection modality. Electrochemical detection, for instance when applied to biology (we provide in the Supporting Information the example of reuptake of neurotransmitters), *in vivo* or *in vitro*, usually occurs in the absence of significant convection; hence, the dispersion related component of the IF should be cancelled.

If we consider that the input concentration signal S_{in} is first distorted by Taylor dispersion in the fluidic circuit, and then by the mechanisms of the electrochemical detection, we can associate two new IFs, characteristic for each of these independent phenomena, IF_d and IF_e, for the fluidic dispersion and the electrochemical detection, respectively. The dispersion profile is the same for all the detection protocols, so IF_d does not change with the electrochemical method, but IF_e is expected to be characteristic of each detection scheme. By taking advantage of the associativity of the convolution operation, we can write that the output signal S_{out} (in this case, the measured current) is obtained from the input signal S_{in} (here, the concentration of analyte close to the electrode) with

$$S_{oot}(t) = (S_{ii} * II_d) * II_e(t)$$

$$= S_{ii} * (II_d * II_e)(t) \qquad (5)$$

Therefore, the IFs presented on Fig. 5C are actually the convolutions of IF_d and IF_e. As no significant electrochemical delaying effect is expected to occur during AMP detection, because of the developed diffusion layer established during this type of detection, the signal distortion can be solely attributed to dispersion, so that IF_d can be safely taken as IF_{AMP} (where IF_{AMP} is the IF associated to AMP). Hence, the IF_e for each chosen potential waveform can be easily obtained by recording and deconvoluting IF_{AMP} from the IFs obtained from the step data. The resulting IF_es are shown on Fig. 6A, with the associated MTFs on Fig. 6B. This shows again that the time response of the CV increases with η. These new IF_es, separated from the effects of dispersion of the analyte plug, can be used to process some analytically relevant electrochemical data in the absence of convection. This method however still shows some inaccuracies, mostly because the diffusive relaxation depends on δ_D (see eqn. (1)) which is itself controlled by v.

Therefore the IF_e is partly diffusion-dependent, but this effect is still expected to be minimal in comparison to the effect of dispersion.

4. Conclusions

The effect of the relaxation time of the diffusion layer on the temporal response of potentiodynamic methods was investigated, showing that the best measurements were obtained for the waveform allowing the most advanced development of the concentration gradient and therefore of the diffusion layer. In all the cases, AMP shows the best time response, but if the ability to detect simultaneously different analytes is important to the experimental design, then voltammetry has to be used, to take advantage of its high chemical resolution. In this case, the potential waveform can be tuned to improve the time response of the system. In this report, where oxidation was analysed, this corresponds to a waveform with a long oxidation, and a short reduction region. However, if a reduction is to be studied, the opposite case (long reduction, short oxidation) will provide the best result. These phenomena should therefore be taken into account when a fast response time is needed, or when precise temporal measurements are important. Practically, using an extended potential waveform (higher anodic limit) [37,38] or a 'sawhorse' waveform [39], showing a plateau at the anodic limit, would also both help improving the temporal response.

5. Acknowledgements

Funding of this work was provided by the EPFL, the EU Ideas program (ERC-2012-AdG-320404). The authors thank the staff of the Center of Micro- and Nanotechnology of EPFL for assistance in the micro-fabrication processes.

6. Supporting Information

A file of Supporting Information is available, providing details on: finite element modelling of the system; experimental procedure; MTF; derivation of the equation describing the CA behaviour; SD of the experimental data; example of the reuptake of neurotransmitters.

7. References

[1] J. Wang, Electrochemical detection for microscale analytical systems: a review, Talanta. 56 (2002) 223.

[2] W. Siangproh, W. Dungchai, P. Rattanarat, O. Chailapakul, Nanoparticle-based electrochemical detection in conventional and miniaturized systems and their bioanalytical applications: A review, Anal. Chim. Acta. 690 (2011) 10.

[3] E. Kätelhön, B. Wolfrum, On-chip redox cycling techniques for electrochemical detection, Rev. Anal. Chem. 31 (2012) 7. [4] D. O'Hare, Biosensors and Sensor Systems, in: G.-Z. Yang (Ed.), Body Sensor Network, Springer, London, 2014, p. 55.

[5] M. Datta, D. Landolt, Fundamental aspects and applications of electrochemical microfabrication, Electrochimica Acta. 45 (2000) 2535.

[6] H. Suzuki, Advances in the Microfabrication of Electrochemical Sensors and Systems, Electroanalysis. 12 (2000) 703.

[7] J. Wang, Electrochemical biosensors: Towards point-of-care cancer diagnostics, Biosens. Bioelectron. 21 (2006) 1887.

[8] A.P.F. Turner, Biosensors: sense and sensibility, Chem. Soc. Rev. 42 (2013) 3184.

[9] R.G. Compton, A.C. Fisher, R.G. Wellington, P.J. Dobson, P.A. Leigh, Hydrodynamic voltammetry with microelectrodes: channel microband electrodes; theory and experiment, J. Phys. Chem. 97 (1993) 10410.

[10] M. Thompson, R.G. Compton, Voltammetric Monitoring of Transient Hydrodynamic Flow Profiles in Microfluidic Flow Cells, Anal. Chem. 79 (2007) 626.

[11] C. Amatore, N. Da Mota, C. Lemmer, C. Pebay, C. Sella, L. Thouin, Theory and Experiments of Transport at Channel Microband Electrodes under Laminar Flows. 2. Electrochemical Regimes at Double Microband Assemblies under Steady State, Anal. Chem. 80 (2008) 9483.

[12] C. Amatore, N. Da Mota, C. Sella, L. Thouin, Theory and Experiments of Transport at Channel Microband Electrodes under Laminar Flows. 1. Steady-State Regimes at a Single Electrode, Anal. Chem. 79 (2007) 8502.

[13] M. Rogers, C. Leong, X. Niu, A. de Mello, K.H. Parker, M.G. Boutelle, Optimisation of a microfluidic analysis chamber for the placement of microelectrodes, Phys. Chem. Chem. Phys. 13 (2011) 5298.

[14] R.G. Compton, P.R. Unwin, Channel and tubular electrodes, J. Electroanal. Chem. Interfacial Electrochem. 205 (1986) 1.

[15] J.A. Cooper, R.G. Compton, Channel Electrodes — A Review, Electroanalysis. 10 (1998) 141.

[16] N.P.C. Stevens, K.A. Gooch, A.C. Fisher, Computational Electrochemistry. Simulations of Homogeneous Chemical Reactions in the Confluence Reactor and Channel Flow Cell, J. Phys. Chem. B. 104 (2000) 1241.

[17] R. Trouillon, Y. Lin, L.J. Mellander, J.D. Keighron, A.G. Ewing, Evaluating the diffusion coefficient of dopamine at the cell surface during amperometric detection: disk vs ring microelectrodes, Anal. Chem. 85 (2013) 6421.

[18] R. Trouillon, A.G. Ewing, Amperometric measurements at cells support a role for dynamin in the dilation of the fusion pore during exocytosis, Chemphyschem. 14 (2013) 2295.

[19] E.V. Mosharov, D. Sulzer, Analysis of exocytotic events recorded by amperometry, Nat. Methods. 2 (2005) 651.

[20] R.M. Wightman, T.J. Schroeder, J.M. Finnegan, E.L. Ciolkowski, K. Pihel, Time course of release of catecholamines from individual vesicles during exocytosis at adrenal medullary cells, Biophys. J. 68 (1995) 383.

[21] W. Harreither, R. Trouillon, P. Poulin, W. Neri, A.G. Ewing, G. Safina, Carbon Nanotube Fiber Microelectrodes Show a Higher Resistance to Dopamine Fouling, Anal. Chem. 85 (2013) 7447.

[22] L.J. Mellander, R. Trouillon, M.I. Svensson, A.G. Ewing, Amperometric post spike feet reveal most exocytosis is via extended kiss-and-run fusion, Sci. Rep. 2 (2012) 907.

[23] F.-R.F. Fan, J. Kwak, A.J. Bard, Single Molecule Electrochemistry, J. Am. Chem. Soc. 118 (1996) 9669.

[24] F.-R.F. Fan, A.J. Bard, Electrochemical Detection of Single Molecules, Science. 267 (1995) 871.

[25] R. Trouillon, M. Gijs, Delayed voltammetric with respect to amperometric electrochemical detection of concentration changes in microchannels, Lab. Chip. 14 (2014) 2929.

[26] C. Cannes, F. Kanoufi, A.J. Bard, Cyclic voltammetry and scanning electrochemical microscopy of ferrocenemethanol at monolayer and bilayer-modified gold electrodes, J. Electroanal. Chem. 547 (2003) 83.

[27] W. Miao, Z. Ding, A.J. Bard, Solution Viscosity Effects on the Heterogeneous Electron Transfer Kinetics of Ferrocenemethanol in Dimethyl Sulfoxide−Water Mixtures, J. Phys. Chem. B. 106 (2002) 1392.

[28] J.V. Macpherson, P.R. Unwin, Hydrodynamic Modulation Voltammetry with an Oscillating Microjet Electrode, Anal. Chem. 71 (1999) 4642.

[29] J.V. Macpherson, P.R. Unwin, Hydrodynamic Modulation Voltammetry with a Variable-Height Radial Flow Microring Electrode, Anal. Chem. 71 (1999) 2939.

[30] A.J. Bard, R.L. Faulkner, Electrochemical Methods: Fundamentals and Applications, 2nd ed., John Wiley and Sons, Hoboken, NJ, 2001.

[31] L. Prandtl, Über Flüssigkeitsbewegung bei sehr kleiner Reibung, in: Verhandlungen des Dritten Int. Math.-Kongresses, Heidelberg, 1904, A. Krazer (Ed.), Teubner, Lepizig, 1905, p. 484.

[32] R.F. Probstein, Physicochemical Hydrodynamics: An Introduction, 2nd ed., Wiley-Interscience, Hoboken, NJ, 2003. [33] J.E. Baur, R.M. Wightman, Diffusion coefficients determined with microelectrodes, J. Electroanal. Chem. Interfacial Electrochem. 305 (1991) 73.

[34] T. Kambara, Polarographic Diffusion Current Observed with Square Wave Voltage. I. Effect Produced by the Sudden Change of Electrode Potential, Bull. Chem. Soc. Jpn. 27 (1954) 523.

[35] H. Bruus, Theoretical Microfluidics, 1st ed., Oxford University Press, Oxford, 2008.

[36] B.P. Jackson, S.M. Dietz, R.M. Wightman, Fast-scan cyclic voltammetry of 5-hydroxytryptamine, Anal. Chem. 67 (1995) 1115.

.[37] M.L.A.V. Heien, P.E.M. Phillips, G.D. Stuber, A.T. Seipel, R.M. Wightman, Overoxidation of carbon-fiber microelectrodes enhances dopamine adsorption and increases sensitivity, The Analyst. 128 (2003) 1413.

[38] S. Hafizi, Z.L. Kruk, J.A. Stamford, Fast cyclic voltammetry: improved sensitivity to dopamine with extended oxidation scan limits, J. Neurosci. Methods. 33 (1990) 41.

[39] R.B. Keithley, P. Takmakov, E.S. Bucher, A.M. Belle, C.A. Owesson-White, J. Park, R.M. Wightman, Higher Sensitivity Dopamine Measurements with Faster-Scan Cyclic Voltammetry, Anal. Chem. 83 (2011) 3563.

[40] B.J. Venton, K.P. Troyer, R.M. Wightman, Response Times of Carbon Fiber Microelectrodes to Dynamic Changes in Catecholamine Concentration, Anal. Chem. 74 (2002) 539.

Figure Captions

Figure 1: Evidence for diffusive relaxation during electrochemical detection using an electrochemical/ microfluidic chip. A) Schematic of the experimental setup, showing the two syringes actuated by a pump injecting specific flow profiles into the electrochemical/ fluidic chip, having a section of mixing serpentines, a Pt working electrode, and an Ag|AgCl reference electrode completing the electrochemical setup. The insert is a simplified cross section view of the chip, showing the inlet and outlet, as well as the working electrode WE positioned across the sensing chamber, orthogonally to the plane of the chip. B) Scheme of the dynamics of the diffusion layer generated at the surface of the electrode during electroanalysis, as explained in the text. The reaction is here presented by the analyte (the red molecule) being oxidised or reduced into its conjugated form (the blue molecule). C) Comparison of AMP (N= 4 repeats, ± SD) and CV

(N= 4 repeats, ± SD) detection of a 4 s step of 1 mM RuHex in aerated PBS injected into the device at 10 µl s^{-1}. The left part shows the normalised currents, underlining the delayed response of CV. The right part shows the impulse response functions (IF) and the modulation transfer functions (MTFs) associated to the AMP and CV detections of FcMeOH (from ref. [25], N= 7 repeats for AMP and N= 8 repeats for CV) and RuHex in similar conditions (4 s step of 1 mM of analyte in aerated PBS injected into the device at 10 µl s^{-1}).

Figure 2: Setup for the CA experiments. A) Input potential waveform *E* (top) and output current *I* (bottom) for a typical cyclic CA trace (t_c= 100 ms, t_{ox}= 50 ms, t_{red}= 50 ms). The η ratio of this potential profile is 0.5. The black dots indicate the points used for the analysis, *i.e.* the currents corresponding to the end of the oxidation phase. B) Typical *I* trace obtained during a single cycle (t_c= 100 ms, η= 0.5), highlighting the times t_{ox} *and* t_{red} used for calculating η. C) Typical CV performed in 1 mM FcMeOH at 100 mV s^{-1}, showing the steady-state plateau-like regions at 0.1 and 0.4 V vs Ag|AgCl D) Computed concentration profile *c*, normalised to the bulk concentration c_0^*, as a function of *t* and the normal distance to the electrode, *z*, during the first CA cycle (t_c= 100 ms), for η= 0.2 and η= 0.8.

Figure 3: Results of the cyclic CA models and experiments. Theoretical (A-C) and experimental (D-F, average of N= 4 chips) data for the cyclic CA analysis in quiescent solution. A, D) Normalised currents obtained from cyclic CA data performed in quiescent 1 mM FcMeOH in aerated PBS, for different values of η (t_c= 100 ms). For the sake of clarity, the SD are not shown here, but are available in the file of Supporting Information. B, E) Same traces as the ones shown in panels A and D, but plotted as a function of $1/\sqrt{t}$, emphasizing the Cottrell-like behaviour of the measured current. C, F) Variations of α, the slope of the linear relation between the normalized current and $1/\sqrt{t}$, as a function of η. The datapoints were fit to a $\eta^{3/2}$ (solid line), emphasizing the relation between α and η. The experimental data in panel F is shown as average ± SD.

Figure 4: Detection of concentration steps with the cyclic CA modality. A) Cyclic CA detection of 4 s plugs of FcMeOH (v= 5 µl s^{-1}) for different values of η (0.1, 0.5 and 1). The traces were all background-subtracted and normalized. For the sake of clarity, the SD are not shown here, but are available in the Supporting Information. B) The cyclic CA traces were fit to the positive part of erf,

see eqn. (4), and the σ values obtained from this fitting are displayed as a function of η (N=3 chips, ± SD). The solid line is a linear fit emphasizing the linear relation between σ and η.

Figure 5: Effect of the range of potential scanned during CV. A) CV traces, run in 1 mM FcMeOH (SR= 0.5 V s^{-1}, v= 10 µl s^{-1}), for the different potential ranges considered in the text, highlighting the oxidation and reduction regions. B) AMP and CV (for the three different potential ranges, SR= 10 V s^{-1}) traces obtained for the injection of a 4 s plug of 1 mM FcMeOH (average of N= 4 repeats, v= 10 µl s^{-1}). The traces were all background-subtracted and normalized. For the sake of clarity, the SD are not shown here, but are available in the file of Supporting Information. C) IFs and D) MTFs obtained from the traces shown in panel B, for the different electrochemical methods.

Figure 6: Isolating the electrochemical delay from fluidic dispersion. A) IF_e characterizing the signal broadening induced by the relaxation of the diffusion layer obtained from the CV traces performed for different ranges of potential. The dispersion component, described by the AMP curves, was deconvoluted from the CV traces. The IF_e associated to the AMP technique is a Dirac pulse, and is not shown on this graph. B) MTF obtained from the IF_e shown on panel A), for AMP traces and CV performed for different potential ranges.

For Table of Content only

Highlights:

- A microchip is used to measure the time response of electrochemical techniques;
- potentiodynamic methods are delayed over amperometry because of diffusive relaxation;
- this phenomenon dampens the behaviour of the diffusion layer at high frequencies;
- this observation can be used to improve the time response of electrochemical systems.

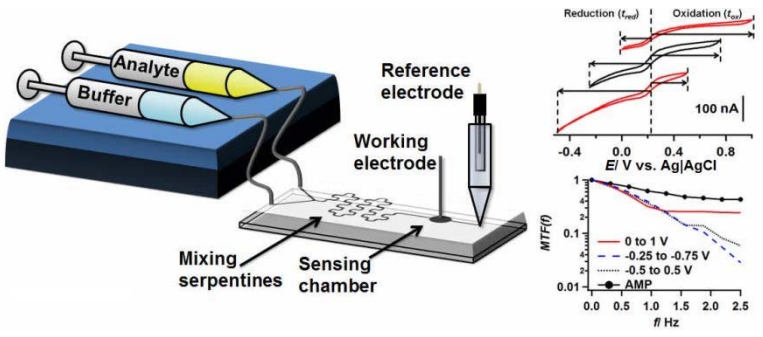

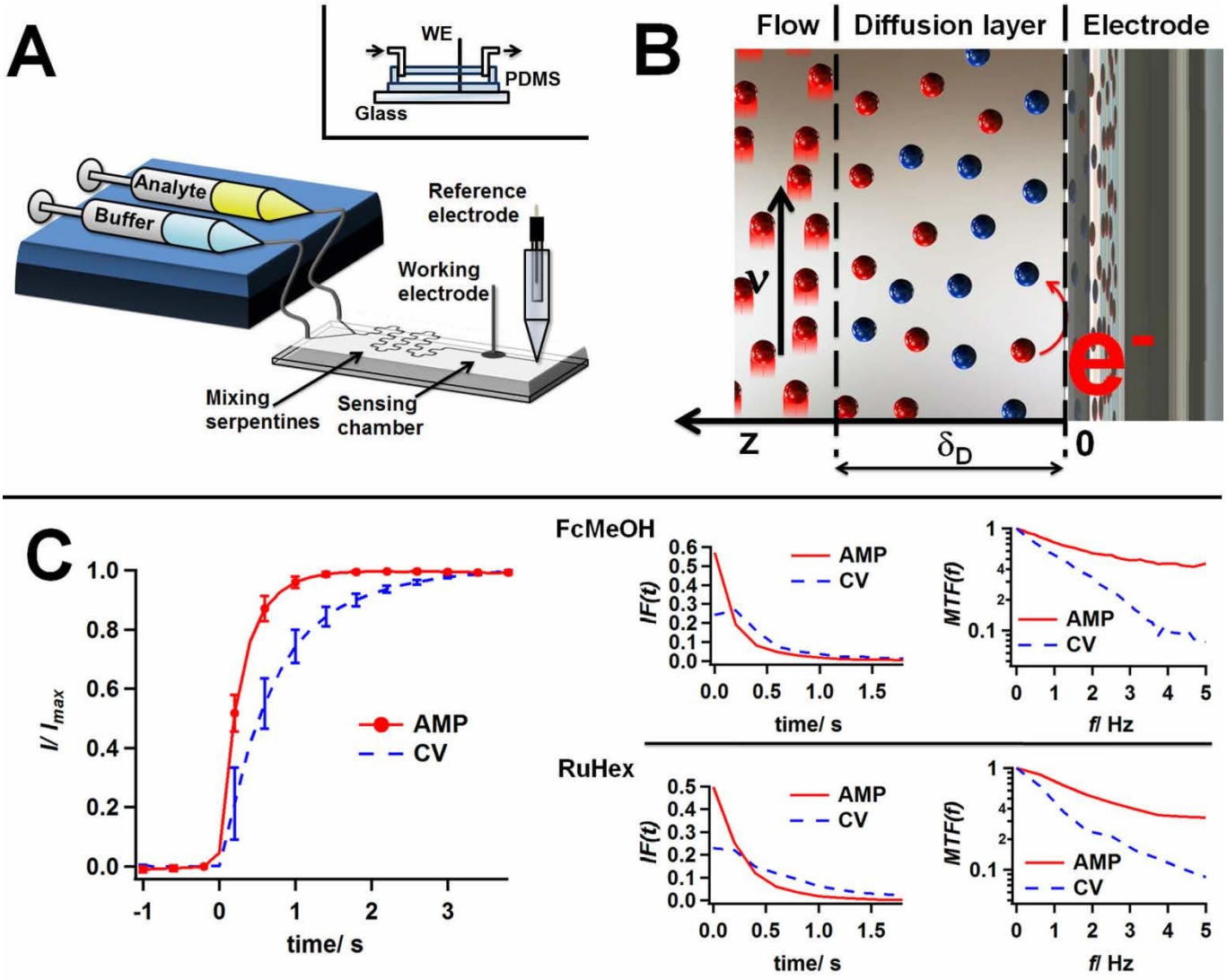
A
WE
PDMS
Glass
Analyte
Buffer
Reference electrode
Working electrode
Mixing serpentines
Sensing chamber
B
Flow
Diffusion layer
Electrode
v
e-
z
δD
0
C
I/ Imax
AMP
CV
time/ s
FcMeOH
IF(t)
MTF(f)
RuHex
f/ Hz

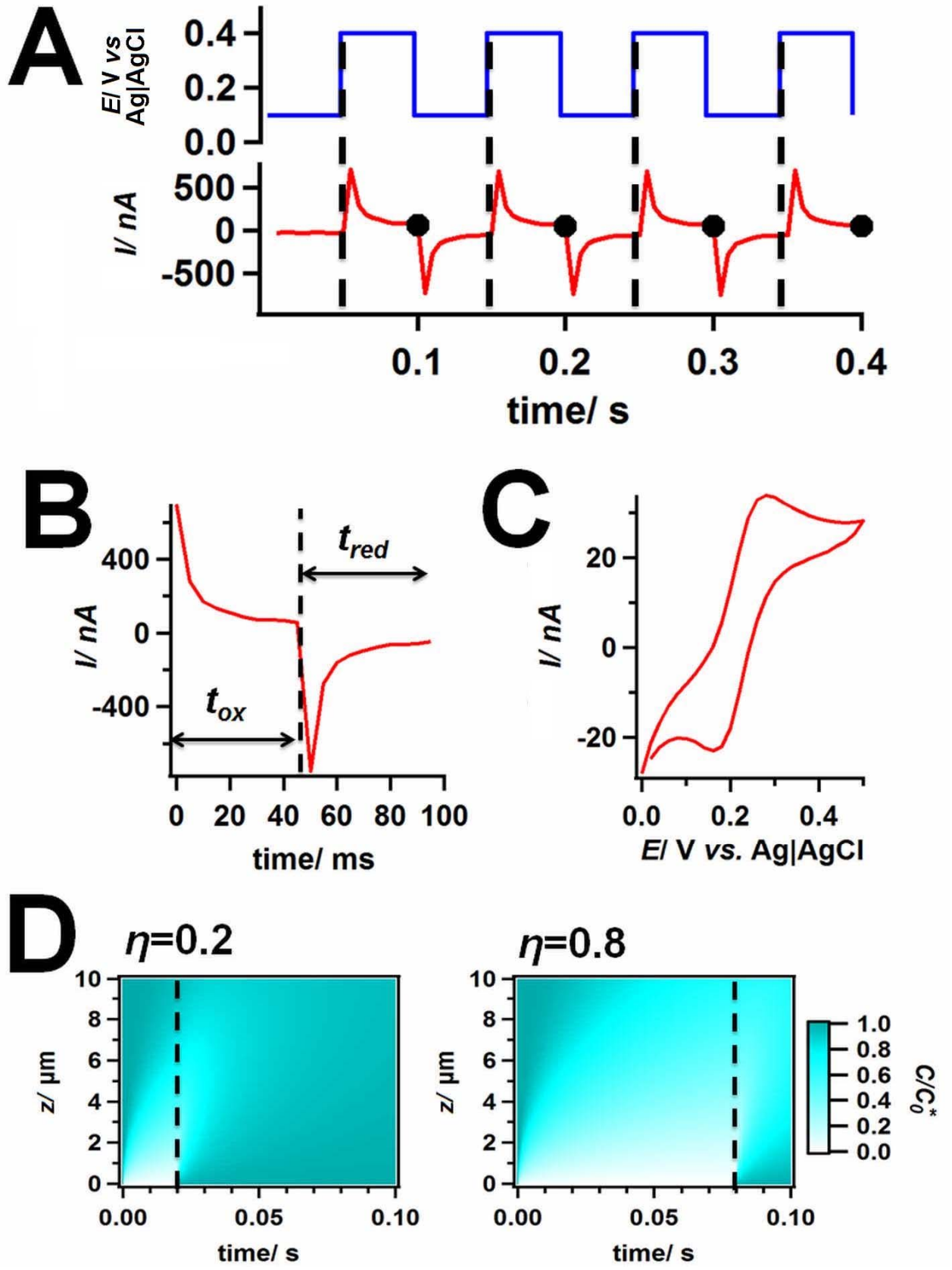
A
E/ V vs Ag|AgCl
0.4
0.2
0.0
I/ nA
500
0
-500
0.1
0.2
0.3
0.4
time/ s
B
400
0
-400
I/ nA
t_red
t_ox
0
20
40
60
80
100
time/ ms
C
20
0
-20
I/ nA
0.0
0.2
0.4
E/ V vs. Ag|AgCl
D
η=0.2
η=0.8
z/ μm
10
8
6
4
2
0
0.00
0.05
0.10
time/ s
1.0
0.8
0.6
0.4
0.2
0.0
C/C0*

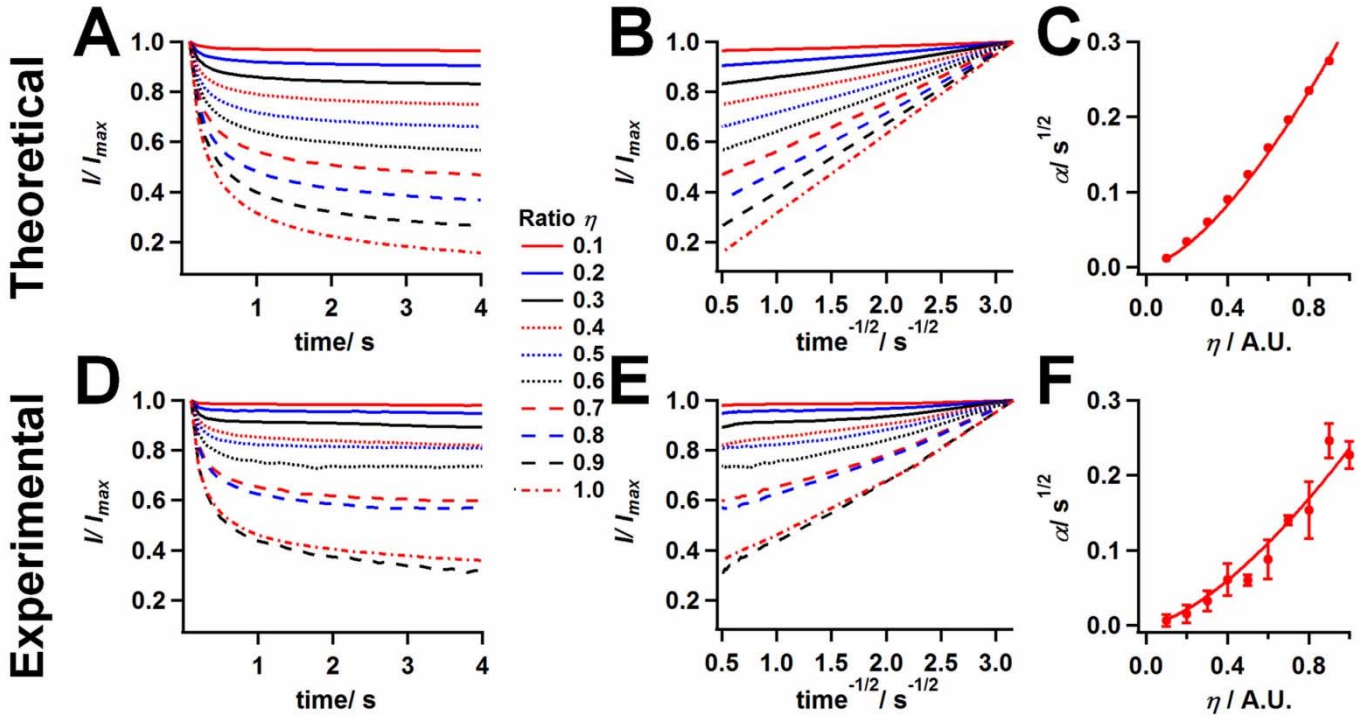
Theoretical
Experimental
A
B
C
D
E
F
I/ I_max
time/ s
time^-1/2 / s^-1/2
αI s^1/2
η / A.U.
Ratio η
0.1
0.2
0.3
0.4
0.5
0.6
0.7
0.8
0.9
1.0

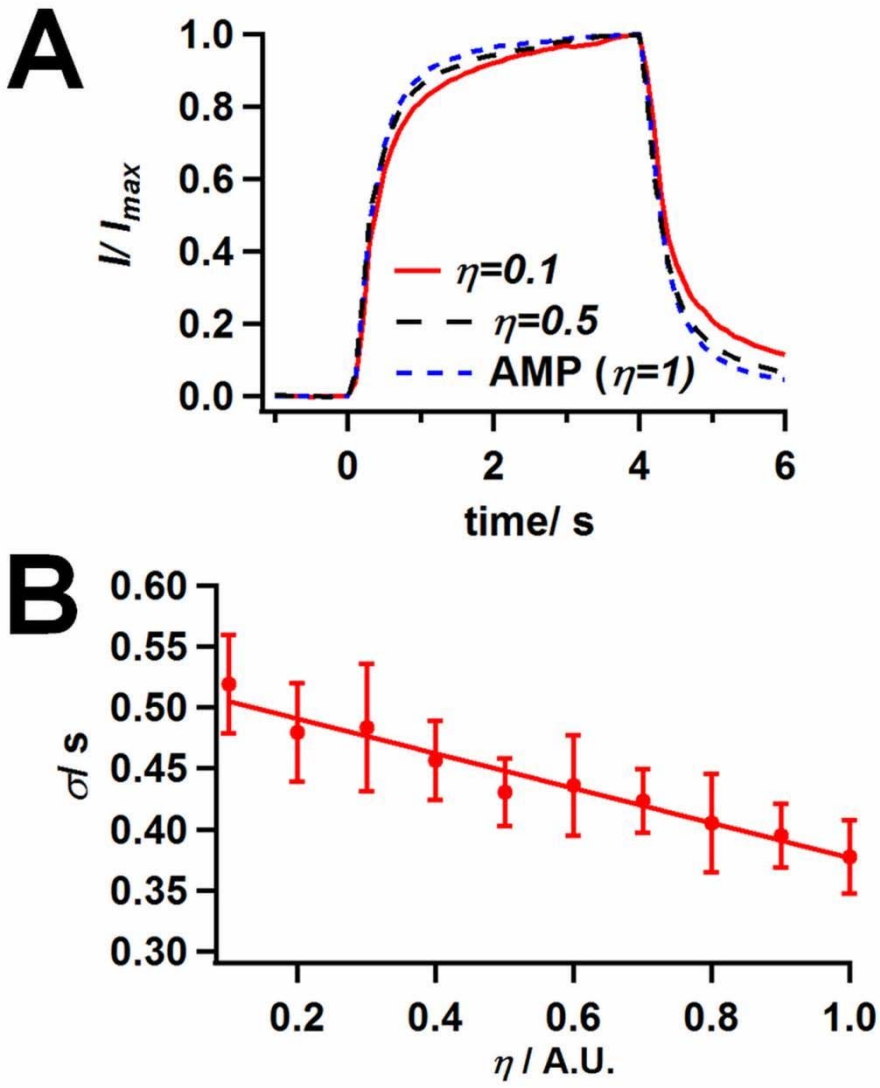
A
1.0
0.8
0.6
0.4
0.2
0.0
I/ I max
η=0.1
η=0.5
AMP (η=1)
0
2
4
6
time/ s
B
0.60
0.55
0.50
0.45
0.40
0.35
0.30
σ s
0.2
0.4
0.6
0.8
1.0
η / A.U.

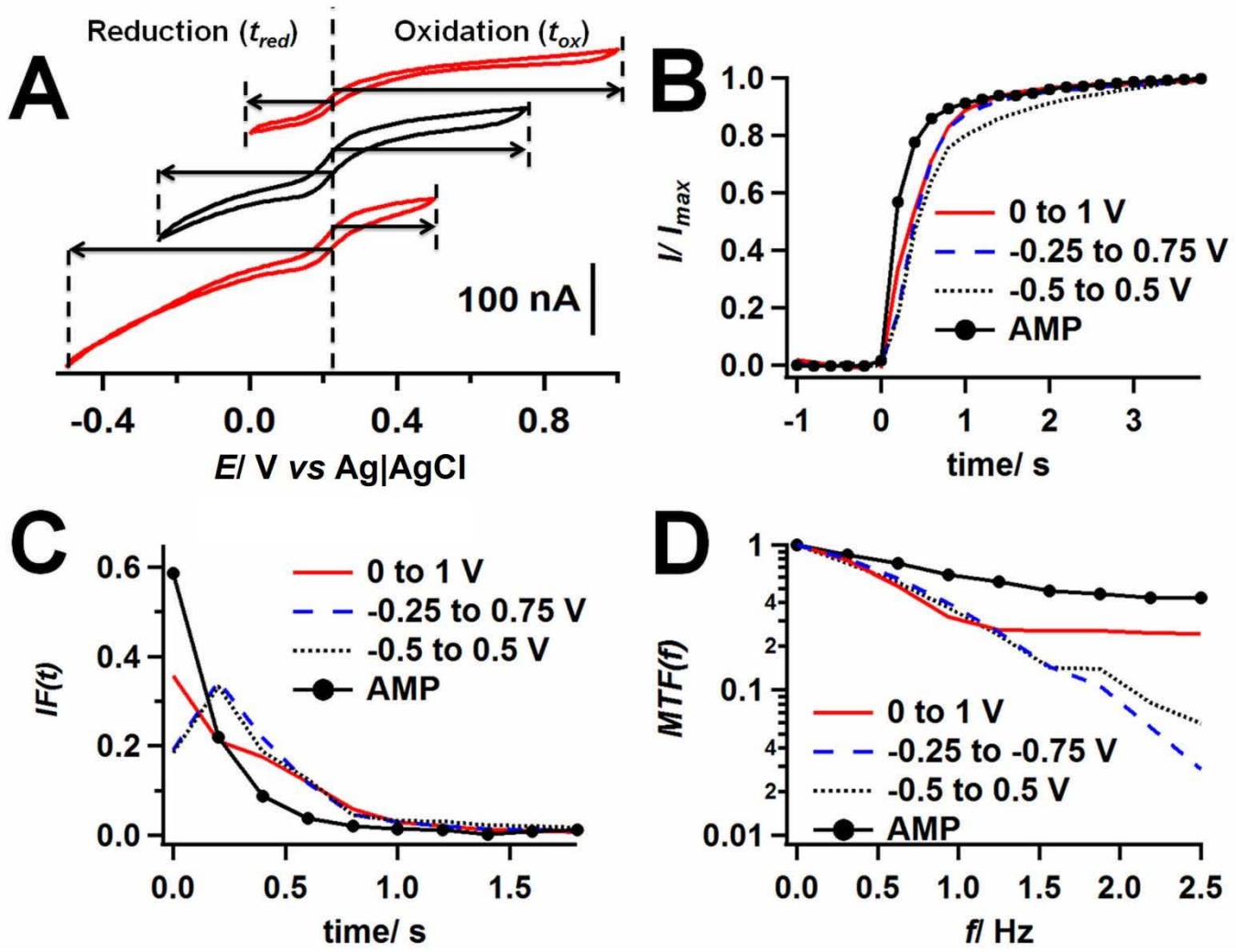
A
Reduction (t_{red})
Oxidation (t_{ox})
100 nA
-0.4
0.0
0.4
0.8
E/ V vs Ag|AgCl
B
I/ I_{max}
1.0
0.8
0.6
0.4
0.2
0.0
-1
0
1
2
3
time/ s
0 to 1 V
-0.25 to 0.75 V
-0.5 to 0.5 V
AMP
C
IF(t)
0.6
0.4
0.2
0.0
0.0
0.5
1.0
1.5
time/ s
0 to 1 V
-0.25 to 0.75 V
-0.5 to 0.5 V
AMP
D
MTF(f)
1
4
2
0.1
4
2
0.01
0.0
0.5
1.0
1.5
2.0
2.5
f/ Hz
0 to 1 V
-0.25 to -0.75 V
-0.5 to 0.5 V
AMP

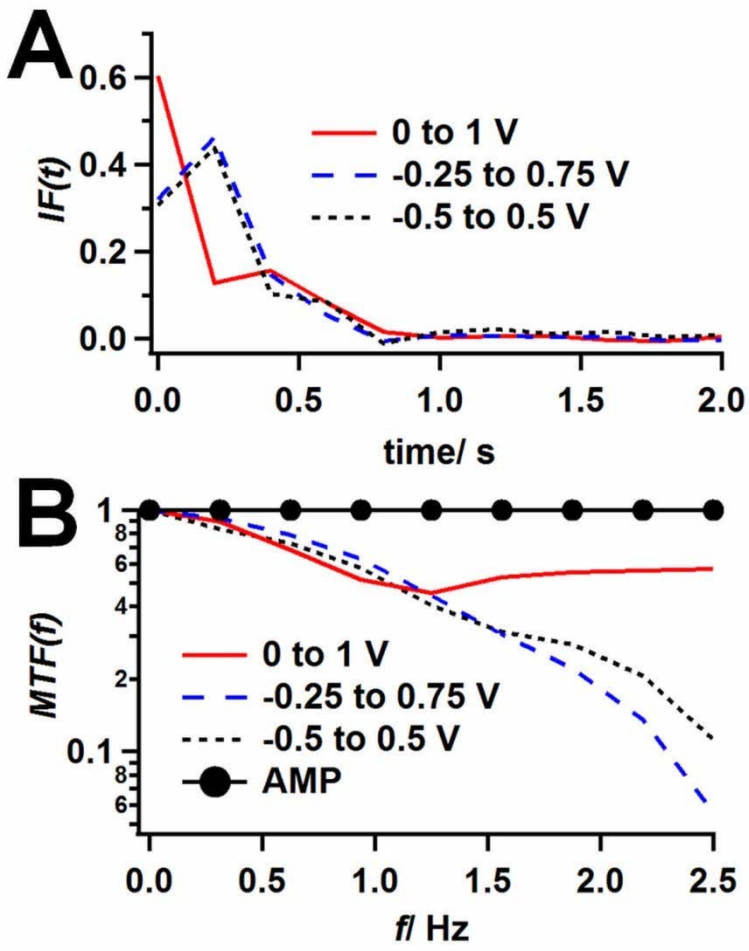
A
0.6
0.4
0.2
0.0
IF(t)
0 to 1 V
-0.25 to 0.75 V
-0.5 to 0.5 V
0.0
0.5
1.0
1.5
2.0
time/ s
B
1
8
6
4
2
0.1
8
6
MTF(f)
0 to 1 V
-0.25 to 0.75 V
-0.5 to 0.5 V
AMP
0.0
0.5
1.0
1.5
2.0
2.5
f/ Hz